NATIONAL ADVISORY COMMITTEE FOR AERONAUTICS

TECHNICAL NOTE 2766

SOME EFFECTS OF AMPLITUDE AND FREQUENCY ON THE AERODYNAMIC DAMPING OF A MODEL OSCILLATING CONTINUOUSLY IN YAW

By Lewis R. Fisher and Walter D. Wolhart

Langley Aeronautical Laboratory
Langley Field, Va.

Washington
September 1952

1H

NATIONAL ADVISORY COMMITTEE FOR AERONAUTICS

TECHNICAL NOTE 2766

SOME EFFECTS OF AMPLITUDE AND FREQUENCY ON THE AERODYNAMIC DAMPING OF A MODEL OSCILLATING CONTINUOUSLY IN YAW

By Lewis R. Fisher and Walter D. Wolhart

SUMMARY

A fuselage—vertical-tail combination was continuously oscillated in yaw through a range of reduced frequencies, which includes the range usually encountered in the lateral oscillations of airplanes, and through a range of amplitudes corresponding to the amplitudes of the sustained lateral oscillation (commonly called snaking) of certain airplanes. The damping in yaw was measured as a phase angle between the lateral force on the vertical tail and the displacement in yaw of the model for each amplitude and frequency condition.

An indication of a reduction in damping in yaw appeared as the amplitude of oscillation was reduced through the range of small amplitudes investigated. The decrease of the lateral damping with reduced-frequency parameter at low frequencies of oscillation was slightly greater than the small variation predicted by the finite-span unsteady-lift theory but not so large as the variation indicated by two-dimensional theory.

INTRODUCTION

Some present-day high-speed airplanes have been found to exhibit in flight an undamped, low-amplitude, lateral oscillation. This instability could logically be explained by a modification of the lateral damping caused by changes in amplitude. In the investigation reported in reference 1, the damping in yaw of a fuselage—vertical-tail combination was determined by the free-oscillation technique in which the amplitude of the motion decreased logarithmically after initial displacement. As a logical extension to that investigation, a similar model was subjected to a constant-amplitude oscillatory motion in yaw in order to establish the effect of a systematic variation of amplitude on the vertical-tail contribution to the damping in yaw. It was further intended to obtain a check on the lateral damping

at low frequencies of oscillation which the results of reference 1 showed to be different from that predicted by two-dimensional theory, but closely in line with the theory in which finite-span effects are considered.

The damping in yaw of the model was determined, for a range of amplitudes and frequencies, as a phase angle between the lateral force on the vertical tail and the displacement in yaw of the model. The measured phase angles were converted analytically to values of the damping-in-yaw parameter which are discussed in relation to the steady-state damping in yaw determined previously by the standard curved-flow procedure used in the Langley stability tunnel.

SYMBOLS

The data are referred to the stability system of axes and are presented in the form of standard NACA coefficients of forces and moments about a point which corresponds to the normal location of the quarter-chord point of the wing mean aerodynamic chord of the model tested. (See fig. 1.) The coefficients and symbols used herein are defined as follows:

a	nondimensional tail length referred to semichord of vertical tail, $-\frac{l_t}{c_t/2}$
A	aspect ratio, b^2/S
b	span, ft
c	chord, ft
$\bar{c}$	mean aerodynamic chord, $\frac{2}{S}\int_0^{b/2} c^2 dy$, ft
f	frequency, cps
I_Z	yawing moment of inertia, ft-lb-sec^2
k	reduced-frequency parameter referred to semichord of vertical tail, $\omega c_t/2V$
l_t	distance from origin of axes to midchord point of vertical tail, ft

N	yawing moment about origin of axes, ft-lb
P	period of oscillation, sec
q	dynamic pressure, $\frac{\rho}{2}V^2$, lb/sq ft
ρ	mass density of air, slugs/cu ft
S	area, sq ft
t	time, sec
V	free-stream velocity, ft/sec
y	spanwise distance from plane of symmetry, ft
α	angle of attack, deg
β	angle of sideslip, radians
$\dot{\beta}$	sideslipping velocity, $d\beta/dt$, radians/sec
ψ	angle of yaw, radians
ψ_o	amplitude
$\dot{\psi}$, r	yawing velocity, $d\psi/dt$, radians/sec
$\ddot{\psi}$	yawing acceleration, $d^2\psi/dt^2$, radians/sec^2
$\omega = 2\pi f$	
ϕ	phase angle between angle of yaw and lift on vertical tail, deg
A,B	functions of k defined in text (see eq. (12))
$C(k) = F + iG$	
F,G	circulation functions used by Theodorsen (ref. 2)
$\overline{P}(k) = F + iG$ $\overline{Q}(k) = H + iJ$	finite-span circulation functions used by Biot and Boehnlein (ref. 3)
C_n	yawing-moment coefficient, N/qS_wb_w

$$C_{n_r} = \frac{\partial C_n}{\partial \frac{rb_w}{2V}}$$

$$C_{n_\beta} = \frac{\partial C_n}{\partial \beta}$$

$$C_{n_{\dot{\beta}}} = \frac{\partial C_n}{\partial \frac{\dot{\beta} b_w}{2V}}$$

$$C_{n_{\dot{\psi}}} = \frac{\partial C_n}{\partial \frac{\dot{\psi} b_w}{2V}}$$

$$C_{n_{\ddot{\psi}}} = \frac{\partial C_n}{\partial \frac{\ddot{\psi} b_w^2}{4V^2}}$$

$$N_\beta = \frac{\partial N}{\partial \beta}$$

$$N_{\dot{\beta}} = \frac{\partial N}{\partial \dot{\beta}}$$

$$N_{\dot{\psi}} = \frac{\partial N}{\partial \dot{\psi}}$$

$$N_{\ddot{\psi}} = \frac{\partial N}{\partial \ddot{\psi}}$$

Subscripts:

t	vertical tail
w	wing

aerod	aerodynamic
meas	measured

APPARATUS

Model

The fuselage of the model was constructed of pine and contained an internal strain-gage side-force balance which was fabricated from sheet aluminum. This balance contained a 4-ounce-capacity Statham strain-gage unit. The dimensions of the model are given in figure 2 and a photograph of the model in the Langley stability tunnel is shown in figure 3. The vertical tail was constructed of balsa wood and was supported by a boom extending rearward from the side-force balance inside the fuselage as shown in figure 3. The effective aspect ratio of the vertical tail was about 2 and the mean chord was 4.9 inches.

Oscillation Apparatus

The model was oscillated continuously through a range of amplitudes and frequencies by the equipment shown in figure 4. A small motor-generator set supplied direct current for a 1-horsepower motor which provided the driving torque through a 6-to-1 speed-reducer gear box. The sinusoidal motion was generated by an eccentric on the gear-box output shaft and transmitted to the model by means of a push rod. The amplitude of the motion was varied by adjusting the throw of the eccentric and the frequency of oscillation was varied by a speed control which governed the output voltage of the motor-generator set. All equipment was mounted outside the test section of the wind tunnel with the exception of the strut upon which the model was mounted. The entire oscillation apparatus was constructed and supported rigidly and built to close tolerances in order to minimize lost motion and low-frequency vibrations which could be transmitted to the recording apparatus.

Recording of Data

A continuous and simultaneous record was made during an oscillation run, at a constant amplitude and frequency, of the tail force, measured by the strain gage, and the model displacement, measured by means of a slide-wire displacement indicator operating on the Wheatstone bridge principle. The data were graphically recorded by an oscillograph which also supplied a continuous time record on the oscillograph paper. In

order to establish as accurate a determination of the lateral damping as possible, while remaining within practical limits of computing time and effort, 50 cycles of motion were recorded for the four highest frequencies of oscillation and 25 cycles were recorded for the three lowest frequencies. Typical traces from the oscillograph record are reproduced in figure 5.

TESTS

The model was oscillated at zero angle of attack with respect to the fuselage center line and in an inverted position in order to minimize any strut interference on the vertical tail. The tests were made with only the fuselage and vertical tail because previous preliminary tests had shown that the wing and horizontal-tail contribution to the lateral damping of this model is negligible at low angles of attack. The oscillation tests were conducted at a dynamic pressure of 24.9 pounds per square foot and a Reynolds number of 442,000 based on the wing mean aerodynamic chord.

The frequencies of oscillation were chosen such that the range of the reduced-frequency parameter $\omega c_t/2V$ encompassed the range commonly encountered in the lateral oscillations of airplanes. The range of amplitudes was chosen to correspond to the amplitudes of the sustained lateral oscillation (snaking) reported in the flight behavior of certain airplanes. The nominal values of the actual frequencies of oscillation were 0.5, 0.7, 1.0, 1.5, 2.0, 3.0, and 4.0 cycles per second, and, for each of these frequencies, the amplitudes of the motion were $1/2^\circ$, 1°, 2°, and 4°.

ANALYSIS

For a system having a single degree of freedom in yaw such that for the stability-axes system, shown in figure 1, the angle of sideslip β is the negative of the angle of yaw ψ, the total instantaneous yawing moment can be expressed as

$$N(t) = \left(I_Z - N_{\ddot{\psi}}\right)\ddot{\psi} - \left(N_{\dot{\psi}} - N_{\dot{\beta}}\right)\dot{\psi} + N_\beta\psi \qquad (1)$$

If the motion be specified as harmonic, as it was for these tests, then

$$\psi = \psi_o \cos \omega t$$

and the total yawing moment will be a harmonic function of time. Making the proper substitutions into equation (1), grouping terms, and putting the entire equation into nondimensional form results in the following expression:

$$C_n(t) = \left\{\left[k^2\left(\frac{b_w}{c_t}\right)^2 C_{n_{\ddot{\psi}}} + C_{n_\beta} - \frac{8k^2 I_Z}{\rho S b_w c_t^2}\right]\cos \omega t + k\frac{b_w}{c_t}\left(C_{n_{\dot{\psi}}} - C_{n_{\dot{\beta}}}\right)\sin \omega t\right\}\psi_o \tag{2}$$

where k is the reduced-frequency parameter $\omega c_t/2V$ referred to the semichord of the vertical tail. The total damping, as was also shown in reference 1, is then the difference between the derivatives $C_{n_{\dot{\psi}}}$ and $C_{n_{\dot{\beta}}}$ and the total directional stability is a combination of the derivatives $C_{n_{\ddot{\psi}}}$ and C_{n_β}. The analytical separation of these derivatives made in reference 1, however, showed that the $C_{n_{\dot{\beta}}}$ part is generally a very small portion of the total damping and that the $C_{n_{\ddot{\psi}}}$ part is generally a very small portion of the directional stability.

The phase angle is the angle the tangent of which is the ratio of the out-of-phase to the in-phase components of an equation of the same form as equation (2) so that

$$\tan \phi = \frac{k\frac{b_w}{c_t}\left(C_{n_r} - C_{n_{\dot{\beta}}}\right)}{k^2\left(\frac{b_w}{c_t}\right)^2 C_{n_{\ddot{\psi}}} + C_{n_\beta} - \frac{8k^2 I_Z}{\rho S b_w c_t^2}} \tag{3}$$

It is apparent that the phase angle will be purely aerodynamic only when the inertia-dependent term in equation (3) is zero. In this case

$$\tan \phi_{aerod} = \frac{k\frac{b_w}{c_t}\left(C_{n_r} - C_{n_{\dot{\beta}}}\right)}{k^2\left(\frac{b_w}{c_t}\right)^2 C_{n_{\ddot{\psi}}} + C_{n_\beta}} \tag{4}$$

and the damping in yaw would then be

$$C_{n_r} - C_{n_{\dot{\beta}}} = \frac{1}{k}\frac{c_t}{b_w}\left[k^2\left(\frac{b_w}{c_t}\right)^2 C_{n_{\dot{\psi}}} + C_{n_\beta}\right]\tan \phi_{aerod} \qquad (5)$$

The measured phase angle, however, includes the term dependent upon the inertia of the vertical tail and its support boom as given by equation (3). In the reduction of data, it was necessary to correct the measured phase angle by subtracting the inertia phase angle to obtain the aerodynamic phase angle from which the damping in yaw $\left(C_{n_r} - C_{n_{\dot{\beta}}}\right)$ could be calculated by equation (5). This correction was accomplished by writing equation (3) as follows:

$$\cot \phi_{meas} = \frac{1}{k}\frac{c_t}{b_w}\frac{k^2\left(\frac{b_w}{c_t}\right)^2 C_{n_{\dot{\psi}}} + C_{n_\beta}}{\left(C_{n_r} - C_{n_{\dot{\beta}}}\right)} - \frac{8kI_Z}{\rho S b_w^2 c_t\left(C_{n_r} - C_{n_{\dot{\beta}}}\right)} \qquad (6)$$

where

$$\cot \phi_{meas} = \cot \phi_{aerod} + \cot \phi_{inertia}$$

Substituting equation (5) into equation (6) results in

$$\cot \phi_{meas} = \cot \phi_{aerod} - \frac{8k^2 I_Z}{\rho S b_w c_t^2\left[k^2\left(\frac{b_w}{c_t}\right)^2 C_{n_{\dot{\psi}}} + C_{n_\beta}\right]} \cot \phi_{aerod} \qquad (7)$$

or, finally,

$$\tan \phi_{aerod} = \left\{1 - \frac{8k^2 I_Z}{\rho S b_w c_t^2\left[k^2\left(\frac{b_w}{c_t}\right)^2 C_{n_{\dot{\psi}}} + C_{n_\beta}\right]}\right\}\tan \phi_{meas} \qquad (8)$$

Reference 1 shows both $C_{n_{\ddot{\psi}}}$ and C_{n_β} to be entirely independent of frequency in the range of frequencies and for the low aspect ratios being considered. It is shown also that the $C_{n_{\ddot{\psi}}}$ portion is so small a part of the total stability that it may be neglected in equation (8) for the type of motion being considered. The directional-stability parameter C_{n_β} was, therefore, derived from a static calibration in which the variation of tail force with static angle of sideslip was determined. This parameter, which refers, for this investigation, only to the vertical tail, can also be calculated quite accurately by consideration of the lift-curve slope of the vertical tail for a suitable effective aspect ratio.

Reduction of basic data.- From the oscillation record (see fig. 5), the time difference between the angle of zero yaw and the tail force at zero yaw, as determined from a static calibration, was read twice for each cycle of motion. The two readings were then averaged to give the time difference for the cycle. The mean time difference for the total number of recorded cycles for each amplitude and frequency condition was converted to a phase angle in degrees by the relationship

$$\phi_{meas} = \frac{\Delta t}{P} \times 360 \tag{9}$$

When the tail force leads the displacement, as is the case for normal positive damping, the phase angle between them is considered to be positive.

Theoretical stability derivatives.- The following expressions for the damping-in-yaw and the directional-stability parameters are derived in reference 1 on the basis of the unsteady-lift theory of reference 2:

$$\left.\begin{aligned} C_{n_r} - C_{n_{\dot{\beta}}} &= -\frac{\pi}{2}\left(\frac{c_t}{b_w}\right)^2 \frac{S_t}{S_w}\frac{B}{k} \\ k^2\left(\frac{b_w}{c_t}\right)^2 C_{n_{\ddot{\psi}}} + C_{n_\beta} &= -\frac{\pi}{2}\frac{c_t}{b_w}\frac{S_t}{S_w} A \end{aligned}\right\} \tag{10}$$

An equation for the phase angle in terms of the unsteady-lift functions A and B can be obtained by combining equations (10) and (4) so that

$$\tan \phi_{aerod} = \frac{B}{A} \tag{11}$$

where, for the infinite-aspect-ratio case,

$$\left.\begin{aligned} B &= -\left(a - \frac{1}{2}\right)k - \left(a + \frac{1}{2}\right)2G + \left(a^2 - \frac{1}{4}\right)2kF \\ A &= \left(a^2 + \frac{1}{8}\right)k^2 + \left(a + \frac{1}{2}\right)2F + \left(a^2 - \frac{1}{4}\right)2kG \end{aligned}\right\} \tag{12}$$

The functions F and G represent the real and imaginary parts, respectively, of the complex Theodorsen unsteady-circulation function C(k). These functions are tabulated in reference 2 and may be computed from expressions given in reference 2 in terms of Bessel functions of the first and second kinds, of orders zero and one, and of the argument k.

The aerodynamic span effect is treated by Biot and Boehnlein in reference 3 and is presented in that reference in closed form as a one-point approximation to the span effect for oscillating surfaces of arbitrary aspect ratio. The method of reference 3 makes use of the finite-span circulation functions

$$\overline{P}(k) = F + iG$$

$$\overline{Q}(k) = H + iJ$$

For infinite aspect ratio

$$\overline{P}(k) = \overline{Q}(k) = C(k)$$

where C(k) is the Theodorsen function. In the notation of reference 3, the factors B and A are

$$\left.\begin{aligned} B &= (2a - 1)akF + \left(a - \frac{1}{2}\right)kH - \left(a - \frac{1}{2}\right)k - 2aG - J \\ A &= (2a - 1)akG + \left(a - \frac{1}{2}\right)kJ + \left(a^2 + \frac{1}{8}\right)k^2 + 2aF + H \end{aligned}\right\} \tag{13}$$

The finite-span functions $\bar{P}$ and $\bar{Q}$ are tabulated in reference 3 for a range of values of the reduced frequency and may be calculated by methods given in that reference. The use of these finite-span functions in equations (13), (11), and (5) will then yield finite-span values for the phase angle and the damping in yaw.

DISCUSSION OF RESULTS

Phase angle.- The results of this investigation are presented in graphical form in figure 6(a) as phase angles between the displacement of the model and the lateral force acting on the vertical tail. Although some scatter occurred for the low-amplitude low-frequency data, a faired curve appears to represent the general phase-angle variation with frequency parameter quite closely. Also shown in figure 6(a) are the calculated effects of the inertia of the vertical tail and its support which were subtracted from the apparent phase angles to give the true aerodynamic phase angles.

The aerodynamic phase angles are compared in figure 6(b) with those calculated by the method outlined previously and presented in reference 3 for an isolated vertical tail of aspect ratio 2. The agreement is excellent for values of the reduced-frequency parameter up to 0.024; these values include most of the range of interest for stability analysis. At higher reduced frequencies, the calculated phase angles appear to be low relative to the experimental aerodynamic phase angles. As a matter of interest, the phase-angle variation with reduced-frequency parameter is also shown for a two-dimensional vertical tail with the same tail length as that for the model tested, and for a two-dimensional tail with zero tail length. The infinite-aspect-ratio tail with the proper tail length gives values of the phase angle that are approximately 50 percent of the calculated phase angles for the tail of aspect ratio 2. For zero tail length, the phase angles are negative, a fact which signifies negative damping, although, at higher values of the reduced-frequency parameter, the theory of reference 2 shows the phase angles to become positive.

The rotation of the vertical tail about an origin of axes from which it is removed gives rise to a lateral velocity at the vertical tail which may, in fact, be interpreted as a time delay l_t/V between the displacement and the tail force. The phase angle resulting from this effect of the geometric tail length is then $\omega l_t/V$, or

$$\phi \approx -57.3ak$$

in degrees. The variation with reduced-frequency parameter of the phase

angle due simply to the geometric tail length of the model tested is also shown in figure 6(b). The indication is that the greater part of the total phase angle, or the lateral damping, is due to the quasi-steady effect of geometric tail length with the remaining portion resulting from the influence of the periodicity of motion.

Probable error of the phase angle.- The deviation from the arithmetic mean of a number n of empirically determined values which is exceeded by not more than 50 percent of the observed values is termed the probable error of the arithmetic mean and is evaluated by the formula

$$\text{Probable error} = 0.6745\sqrt{\frac{\sum(\Delta t - \Delta t_{mean})^2}{n(n-1)}}$$

The probable errors determined for the phase angles of this investigation are shown in figure 6(c). The accuracy of the phase-angle measurements was considerably better for the greater amplitudes and the higher frequencies of oscillation.

Damping in yaw.- The aerodynamic phase angles were converted to the values of the damping-in-yaw parameter by the relationship given previously and are presented in figure 7(a) as values of $C_{n_r} - C_{n_{\dot{\beta}}}$. As the frequency parameter becomes smaller, the values of the damping in yaw decrease, to a small extent, about in the manner predicted by the unsteady-lift theory, although the rate of decrease is between the results calculated for the infinite-span and the finite-span vertical tails. This small decrease in the damping did not appear in the free-oscillation results of reference 1, possibly because insufficient test points were taken at the higher frequencies of the reference tests.

Both the two-dimensional and the finite-span theories indicate that the damping changes sign and goes to positive infinity as k becomes zero. However, the rate of approach to infinity decreases considerably with a decrease in aspect ratio. For a value of k as low as 0.001, the finite-span theory for aspect ratio 2 yields a reasonable value for $C_{n_r} - C_{n_{\dot{\beta}}}$ which is close to the steady-state value shown in figure 7(a). The steady-state C_{n_r} was obtained by the curved-flow testing procedure of the Langley stability tunnel and it corresponds to the $k = 0$ oscillation condition. In comparison, the two-dimensional theory indicates practically zero damping at $k = 0.001$. The greatest loss in damping predicted by the two-dimensional unsteady-lift theory occurs at $0 < k < 0.004$. Although it was not

practicable to obtain test data by the forced-oscillation technique in this very low range of the reduced-frequency parameter, the results of reference 1 indicate that no such loss in damping occurs for the tail of aspect ratio 2 even to as low a value of k as 0.001.

The experimental data show appreciable scatter for the low-frequency small-amplitude tests. When the damping is cross-plotted against amplitude, however, as was done in figure 7(b), a trend appears from the general picture. If it is recognized that the test data for the lowest frequencies and the smallest amplitudes contain the largest inaccuracies and if the data are weighted accordingly, there appears to be, in general, a small decrease in the lateral damping as the amplitude of the motion is reduced from 4° to $1/2^\circ$. While this result cannot be stated conclusively because of the large scatter of the test points which are of prime importance, the general trend of the data supports the concept that the lateral damping may decrease appreciably from the quasi-steady value at amplitudes of oscillation less that 1°.

Probable error in the damping in yaw.- The probable errors determined for the phase angles were converted to the errors in the damping in yaw shown in figure 7(c). The accuracy of the low-frequency small-amplitude data is rather poor. The $C_{n_r} - C_{n_{\dot{\beta}}}$ values, of course, reflected the phase-angle results in that the accuracy of the higher amplitude and higher frequency data was considerably better than the low frequency and amplitude results.

CONCLUSIONS

The following conclusions were drawn from the results of an investigation of the effects of amplitude and frequency on the directional damping of a vertical tail in the presence of a fuselage during continuous forced oscillation in yaw:

1. There is an indication that the damping in yaw is reduced when the amplitude of oscillation is reduced from 4° to $1/2^\circ$.

2. Some reduction occurred in the magnitude of the damping-in-yaw parameter as the frequency was decreased through the range of frequency parameters investigated. The variation of the lateral damping with reduced-frequency parameter was slightly greater than the small effect

predicted by finite-span unsteady-lift theory but not so large as the variation indicated by two-dimensional theory.

Langley Aeronautical Laboratory
National Advisory Committee for Aeronautics
Langley Field, Va., June 3, 1952

REFERENCES

1. Bird, John D., Fisher, Lewis R., and Hubbard, Sadie M.: Some Effects of Frequency on the Contribution of a Vertical Tail to the Free Aerodynamic Damping of a Model Oscillating in Yaw. NACA TN 2657, 1952.

2. Theodorsen, Theodore: General Theory of Aerodynamic Instability and the Mechanism of Flutter. NACA Rep. 496, 1935. (Reprinted 1940.)

3. Biot, M. A., and Boehnlein, C. T.: Aerodynamic Theory of the Oscillating Wing of Finite Span. GALCIT Rep. No. 5, Sept. 1942.

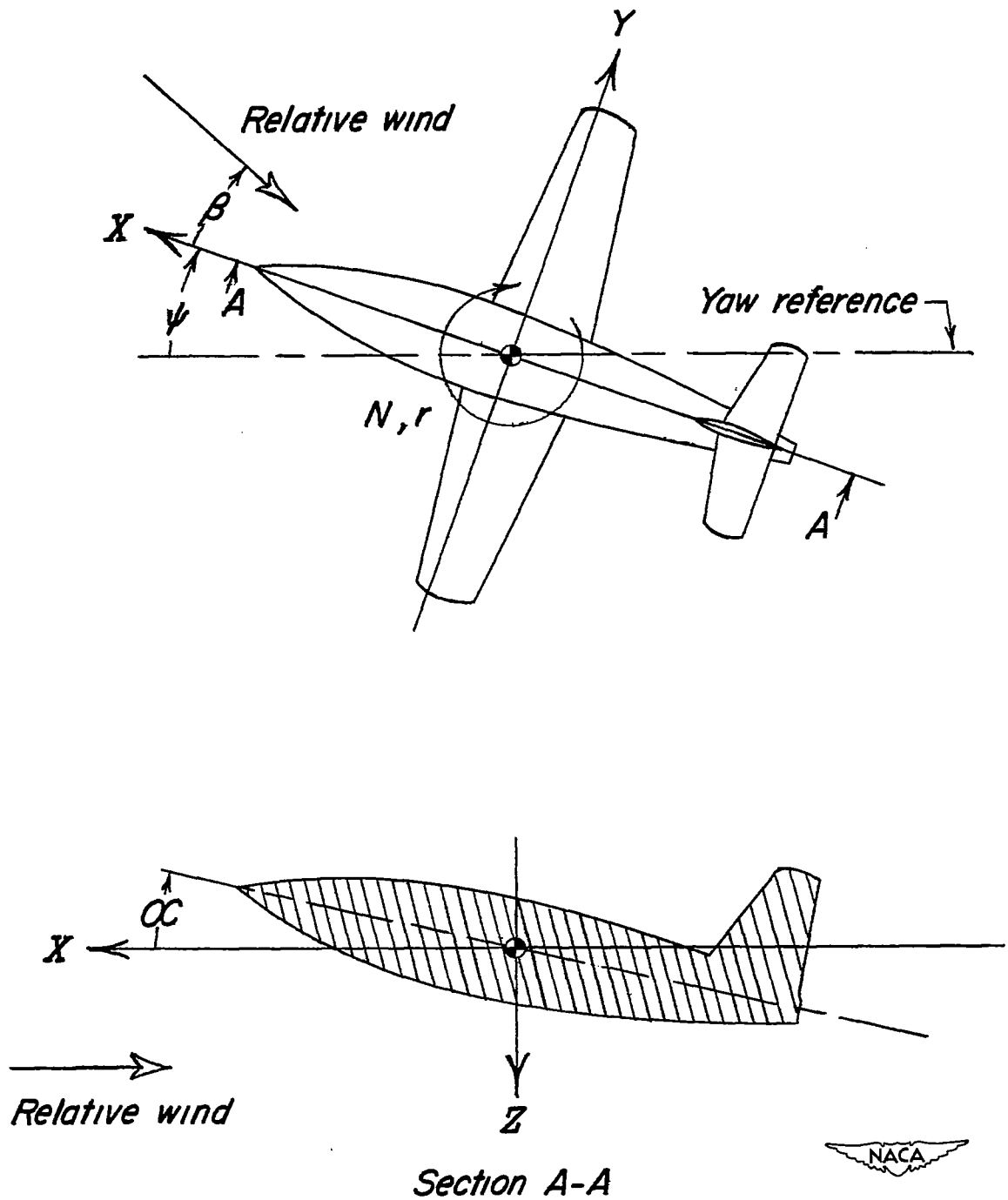

Figure 1.- System of stability axes. Arrows indicate positive forces, moments, and angular displacements. The yaw reference is generally chosen to coincide with the initial relative wind.

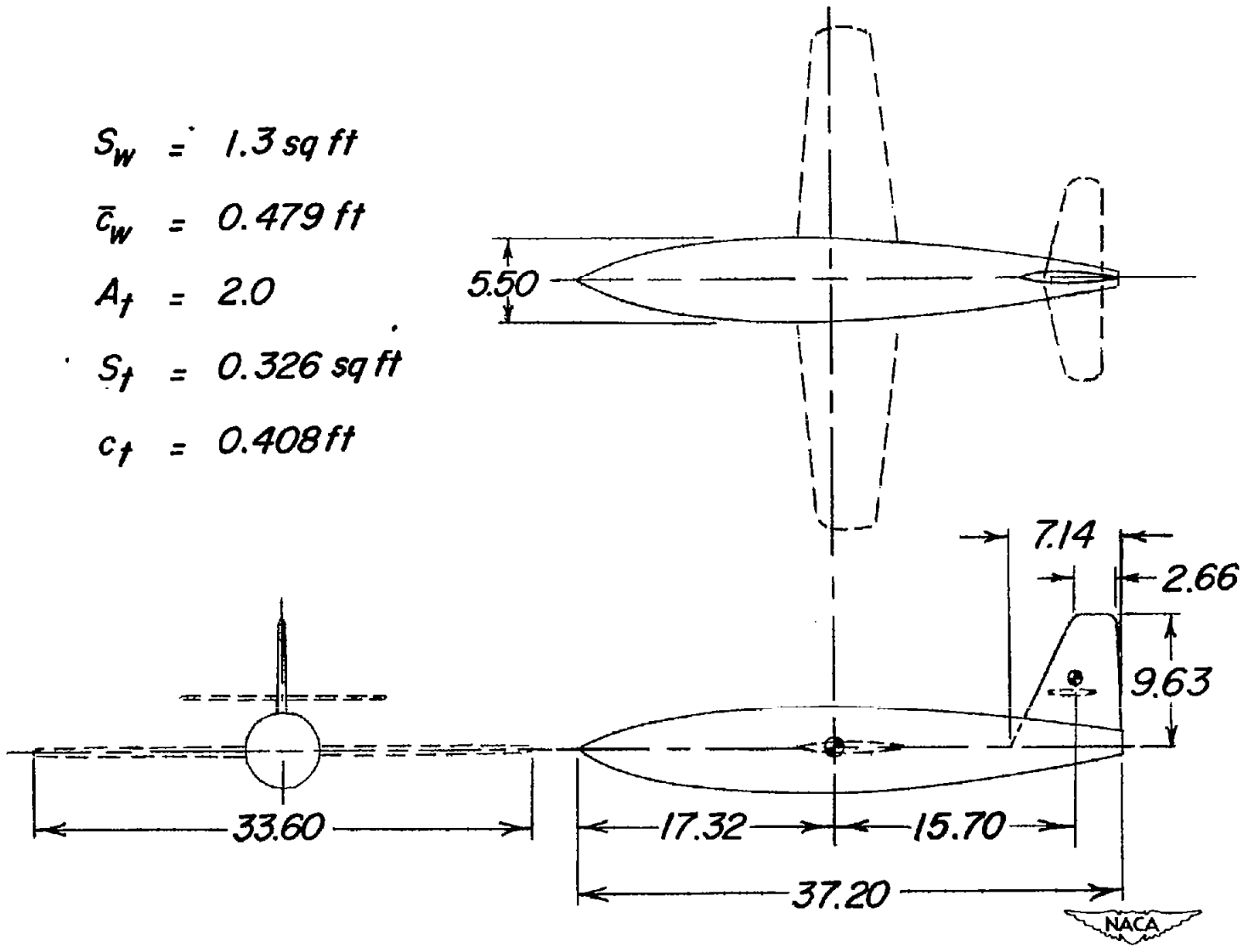

Figure 2.- Model tested. All dimensions are in inches.

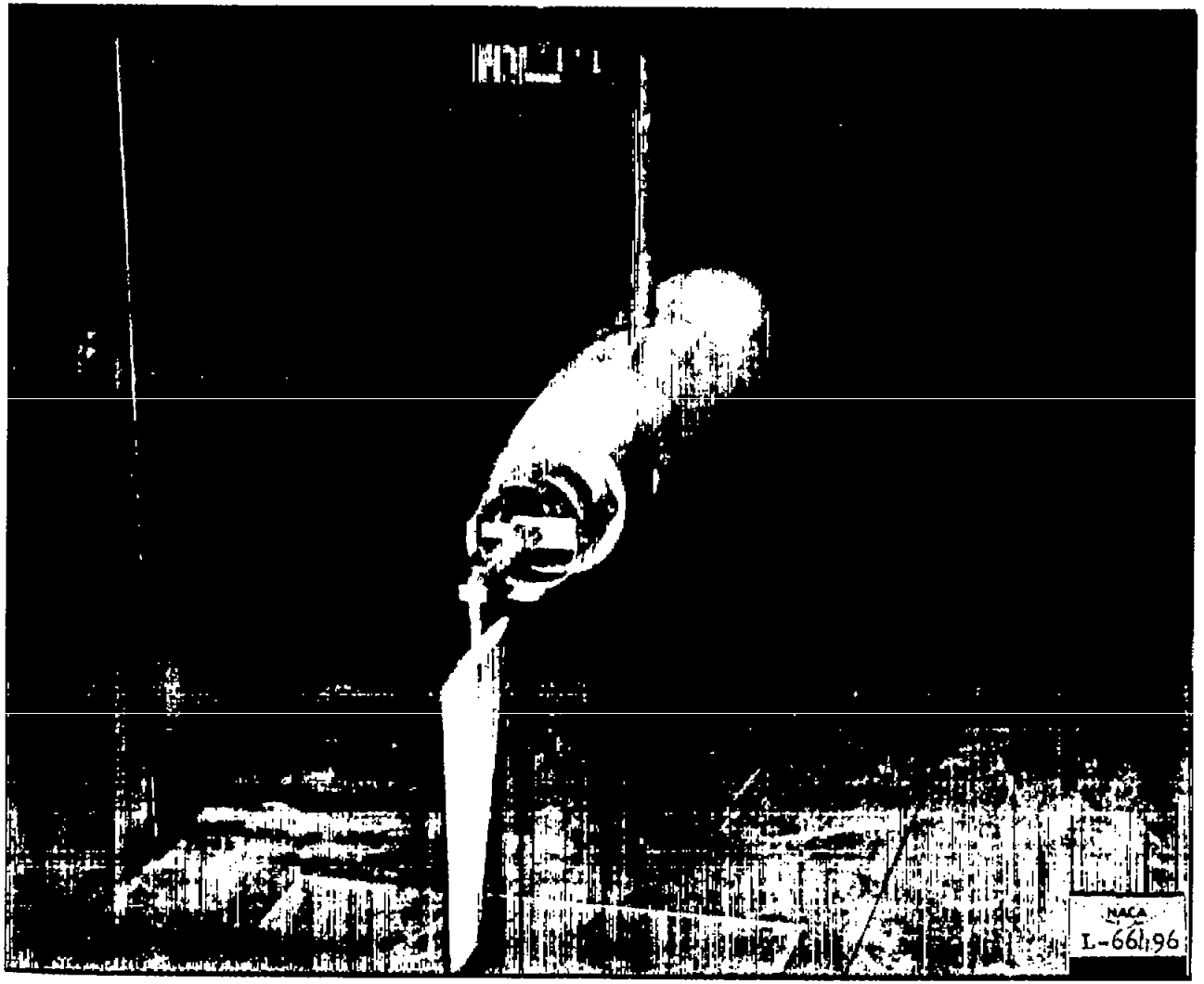

Figure 3.- Oscillation model in Langley stability tunnel. Wing off; tail cone removed to show internal balance.

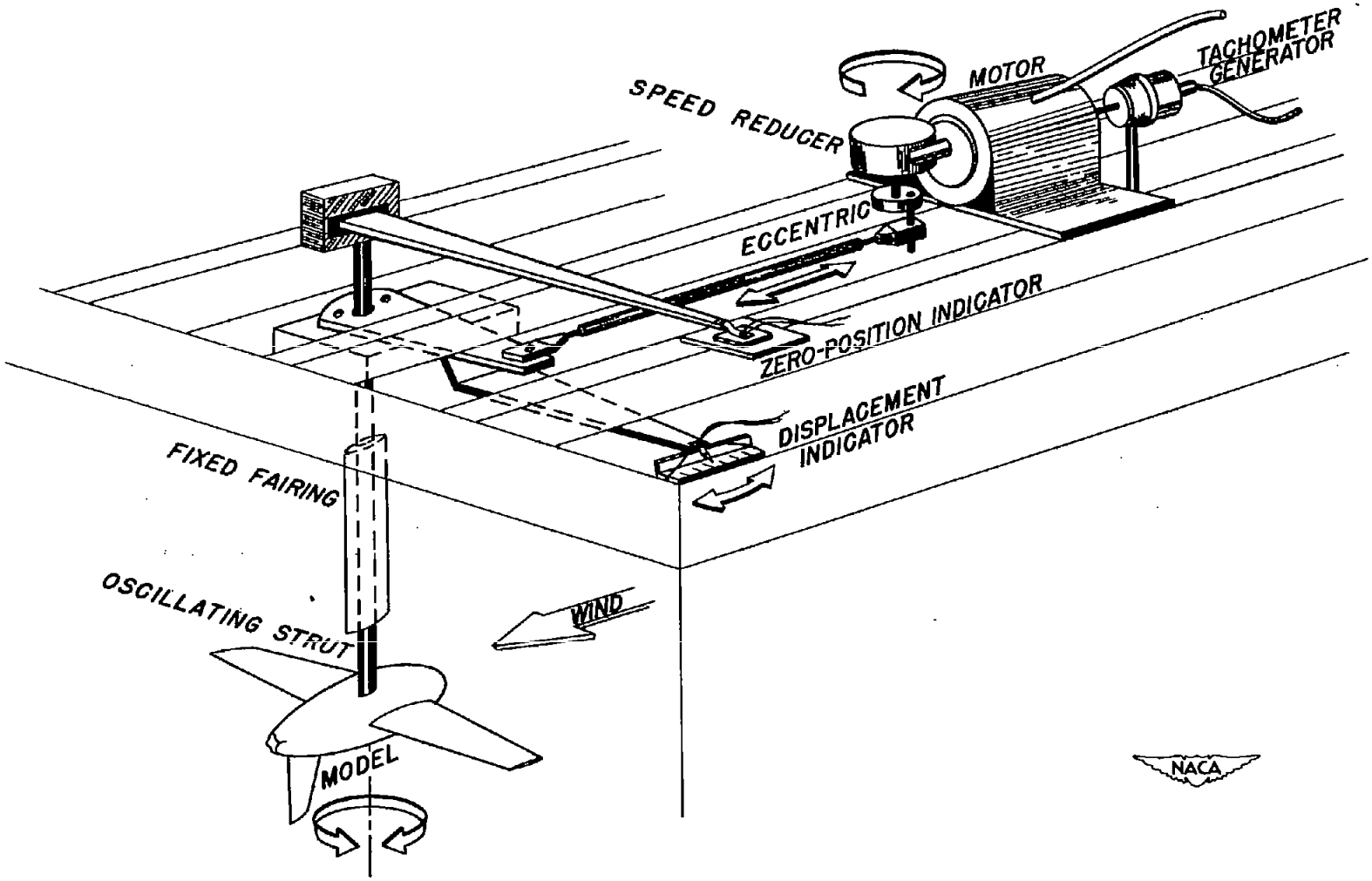

Figure 4.- Oscillation apparatus.

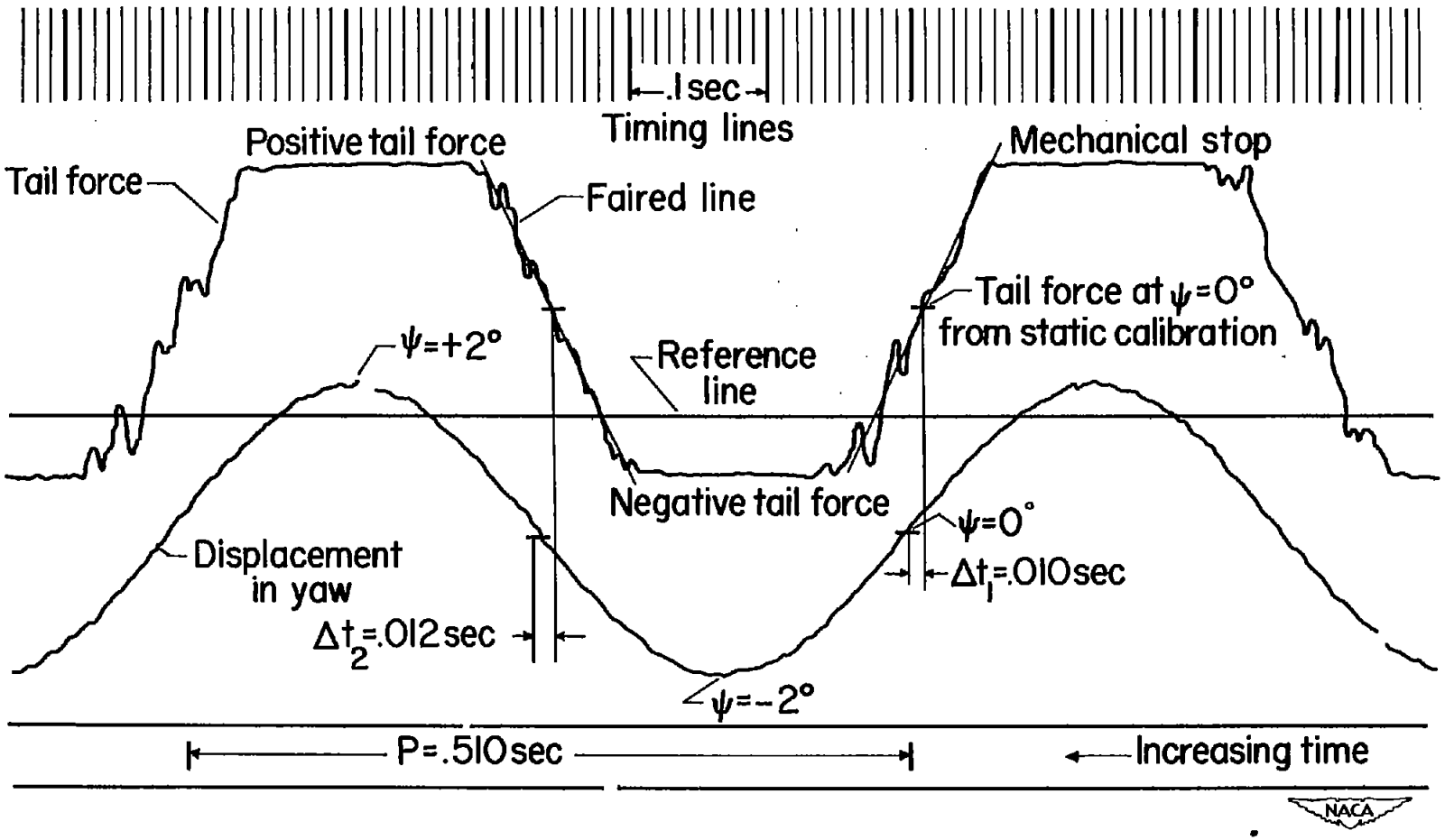

Figure 5.- Typical traces from oscillograph record indicating method of reading time increments. $\Delta t = 0.0110$.

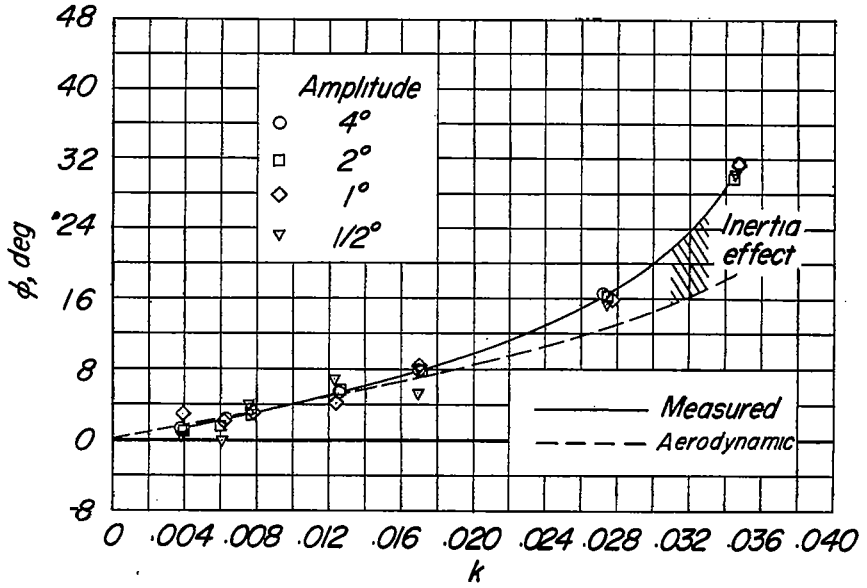

(a) Experimental data and inertia increments.

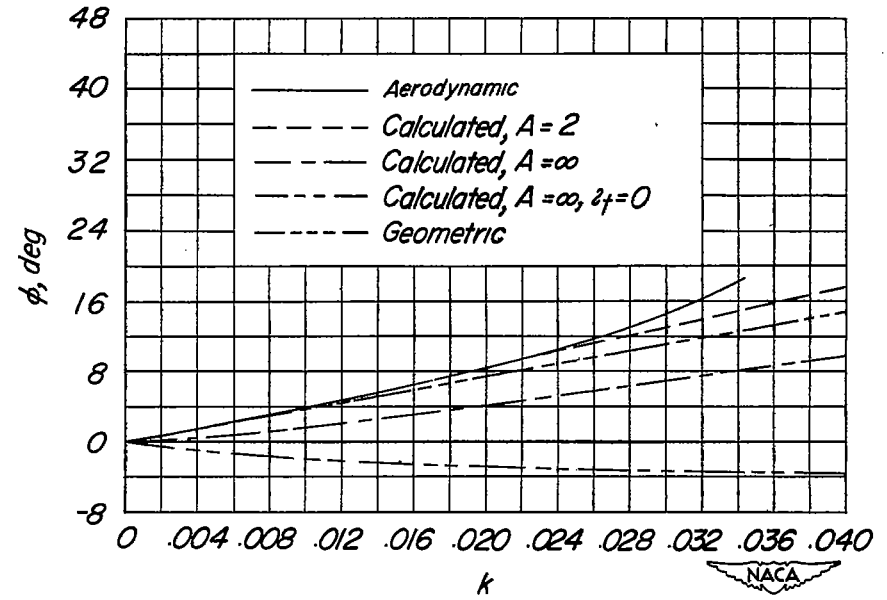

(b) Comparison of experimental aerodynamic phase angles with calculated phase angles indicating some effects of aspect ratio and tail length. l_t = 1.31 feet unless otherwise specified.

Figure 6.- The effect of amplitude and reduced-frequency parameter on the phase angle.

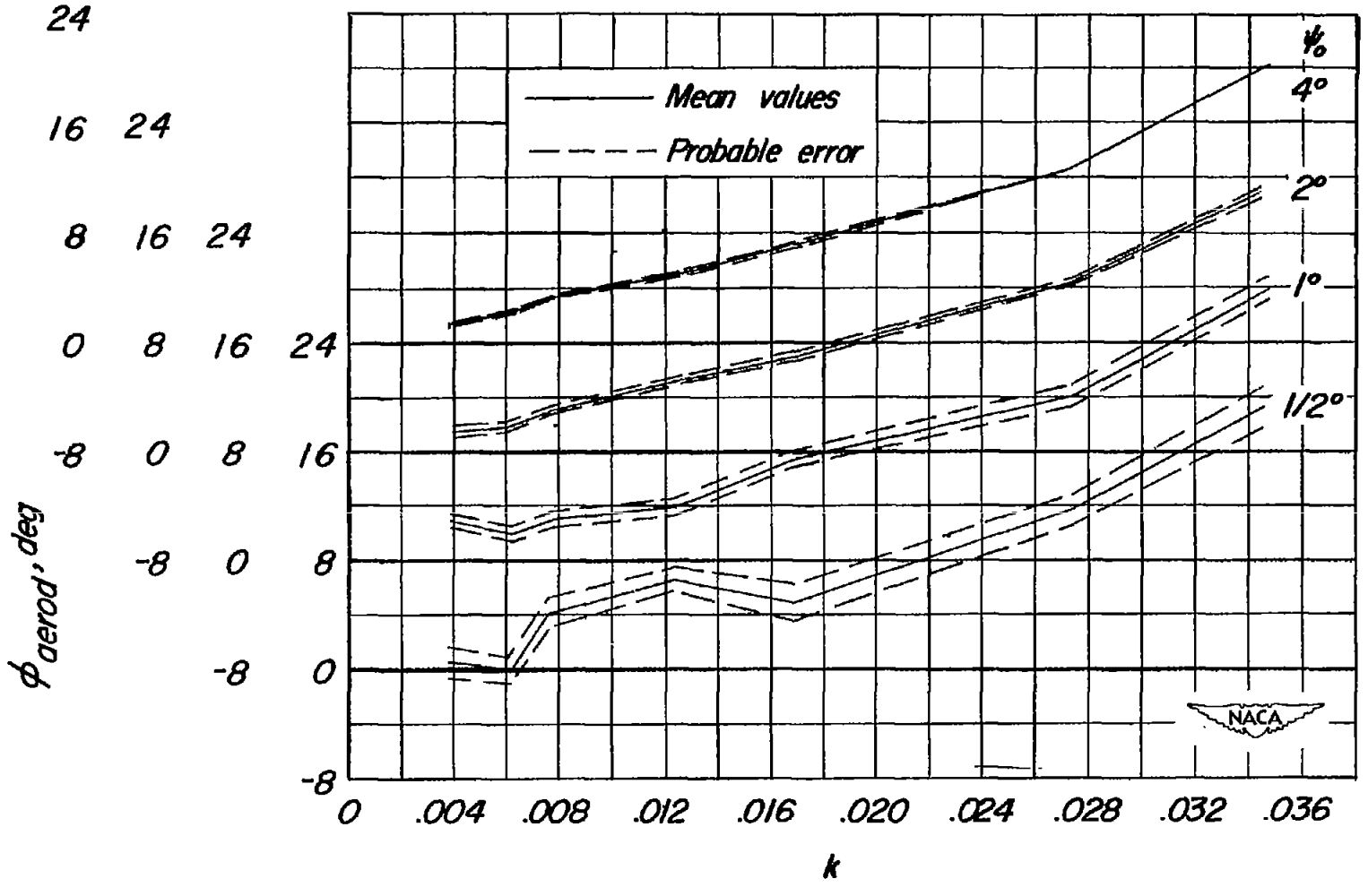

(c) Probable errors of the mean values of aerodynamic phase angles.

Figure 6.- Concluded.

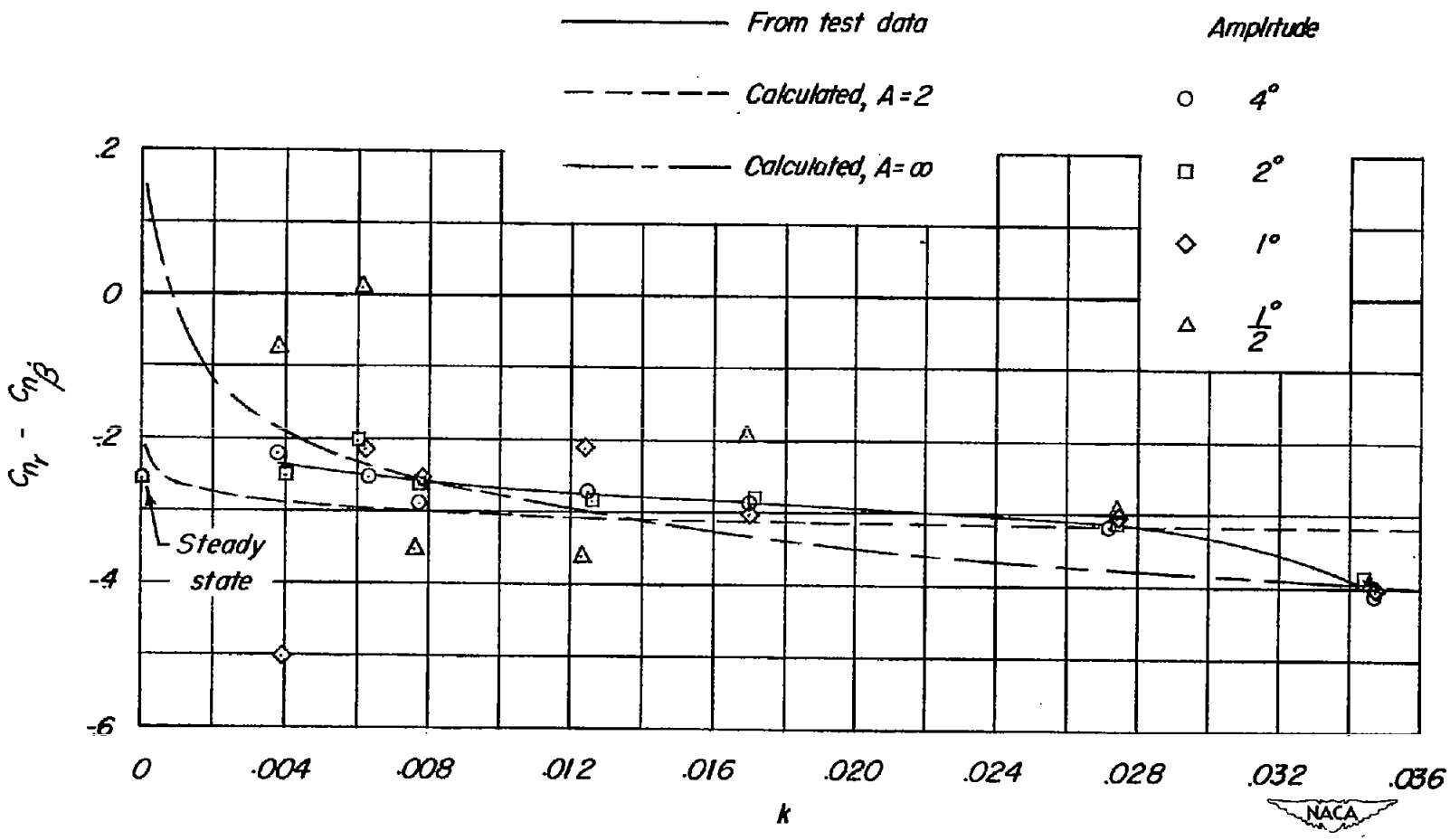

(a) Comparison of measured damping and damping calculated by unsteady-lift theory.

Figure 7.- The effect of amplitude and reduced-frequency parameter on the vertical-tail contribution to the damping in yaw.

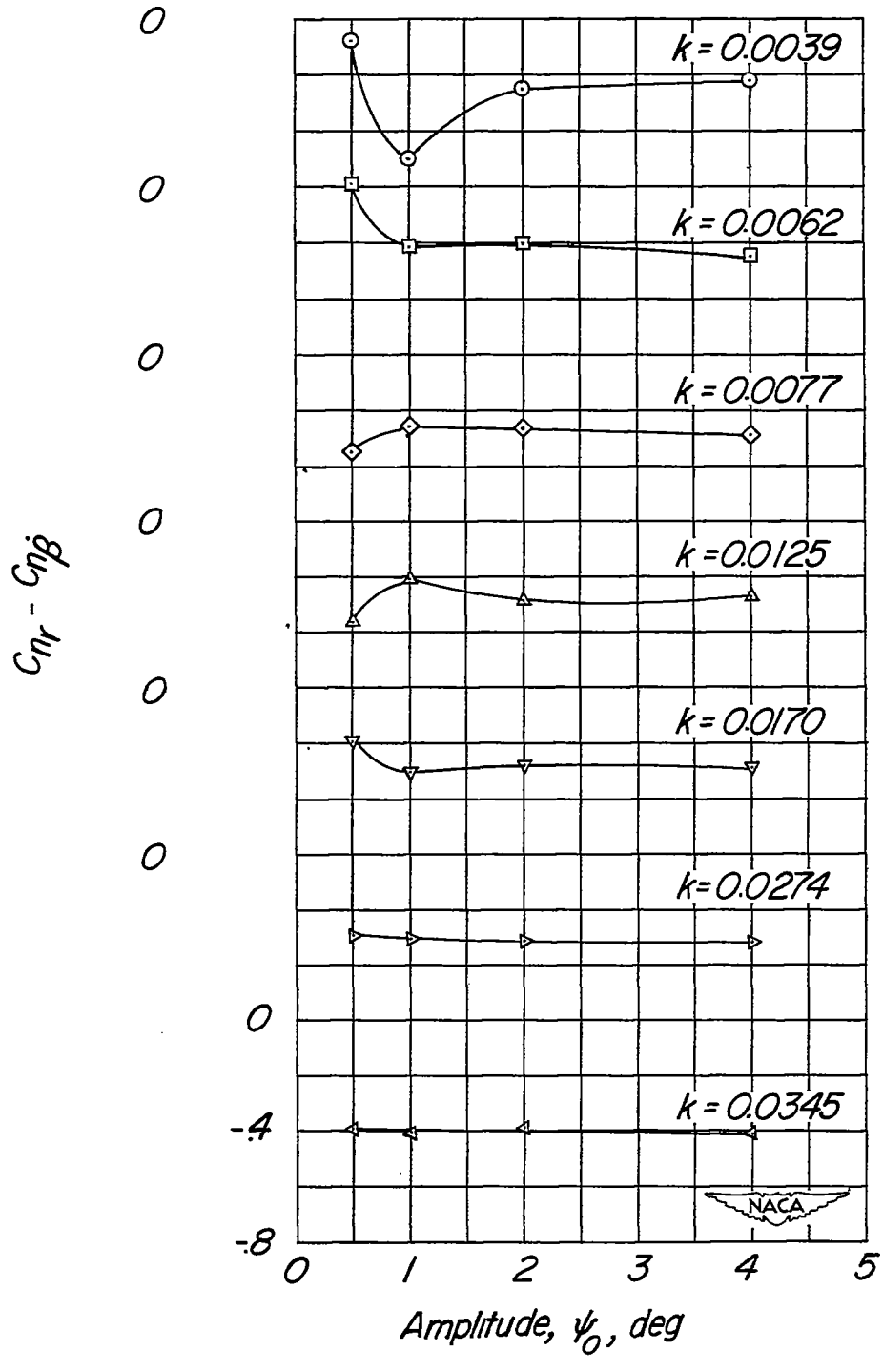

(b) Variation with amplitude of the vertical-tail contribution to the damping in yaw.

Figure 7.- Continued.

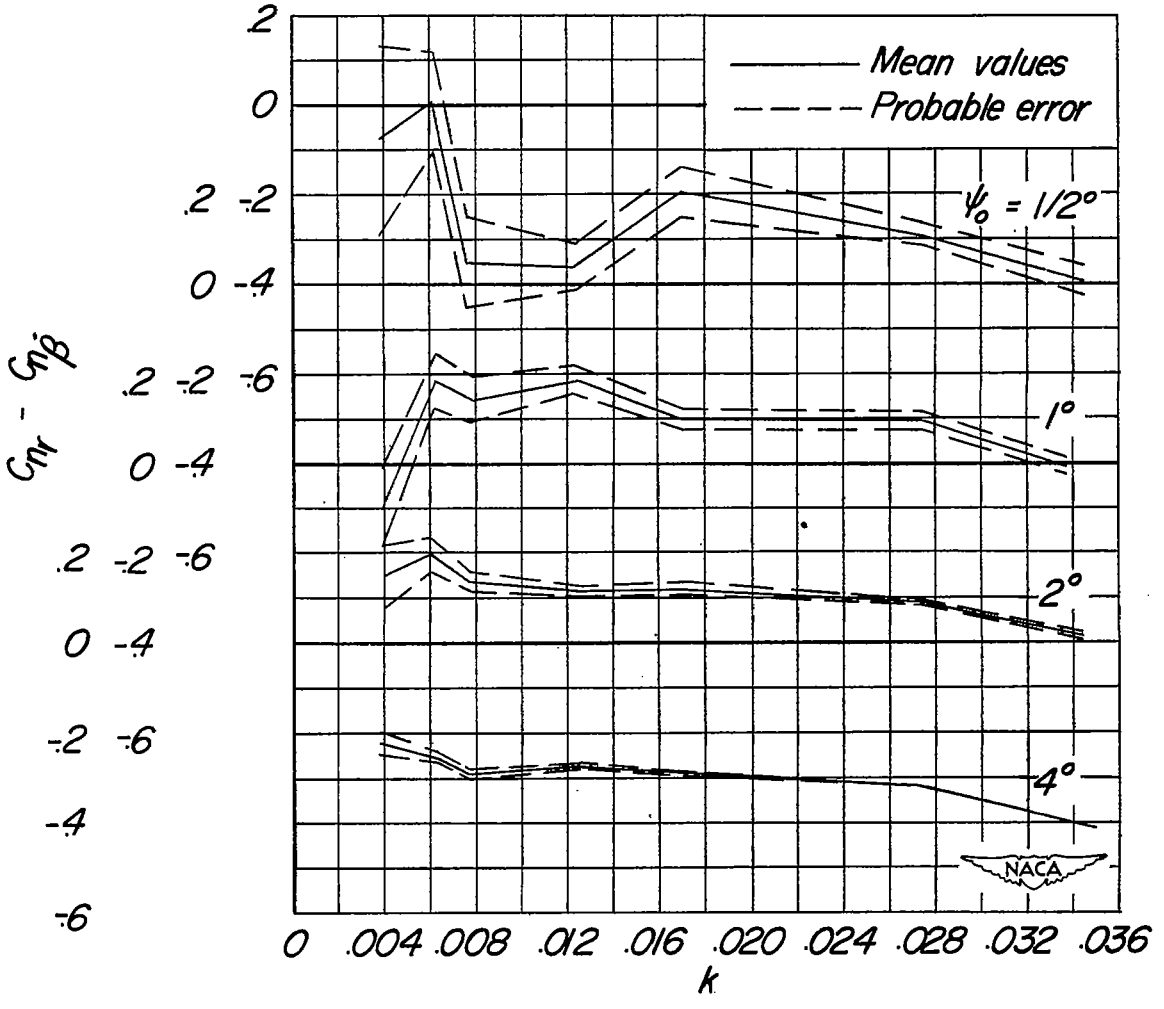

(c) Probable errors of the mean measured values of the damping in yaw.

Figure 7.- Concluded.

NACA-Langley - 9-2-52 - 1000